Nanomanipulation measurement and PIC simulation of field-emission properties from a single crystallized silicon nano-emitter

2007 Nanotechnology 18 225503

(http://iopscience.iop.org/0957-4484/18/22/225503)

Nanotechnology **18** (2007) 225503 (6pp) doi:10.1088/0957-4484/18/22/225503

Nanomanipulation measurement and PIC simulation of field-emission properties from a single crystallized silicon nano-emitter

T C Cheng[1], K H Hsu[2,3], P Y Chen[1,2], W J Huang[1], J S Wu[2], H T Hsueh[1] and M N Chang[1]

[1] National Nano Devices Laboratories, Hsinchu 30078, Taiwan
[2] Mechanical Engineering Department, National Chiao Tung University, Hsinchu 30050, Taiwan
[3] National Space Organization, Hsinchu 30050, Taiwan

E-mail: chongsin@faculty.nctu.edu.tw (J S Wu)

Received 3 March 2007, in final form 6 April 2007
Published 4 May 2007
Online at stacks.iop.org/Nano/18/225503

Abstract
The field-emission characteristics of a single silicon nano-emitter were investigated by means of experiments and simulation models. The emitter array was fabricated by dry etching using an inductively coupled plasma (ICP) through a three-step process. A novel experimental technique was developed to precisely measure the field-emission current from a single silicon emitter. Accompanying these measurements, a parallelized three-dimensional particle-in-cell (PIC) code, in which the Fowler–Nordheim emission law was implemented at the emitter surface, was employed to simulate the emission current both with and without taking into account the space charge effect. Results show that the simulated I–V relationship when considering the space–charge effect was in excellent agreement with the actual measurements. Noticeably, the predicted turn-on voltage was found to be within only 9.3% of the experimental data. In addition, both the predicted and experimental data demonstrated a consistent single linear slope in the FN plot, which indicates that the field emission from a single silicon tip is a barrier-tunnelling, quantum mechanical process.

(Some figures in this article are in colour only in the electronic version)

1. Introduction

Over the past decade, field-emission properties have been studied extensively for various materials and geometrical arrangements, in which performance has been found to strongly depend upon the inherence, morphology [1], material density [2], and the sharpness, aspect ratio and surface conditions of the tip [3–6], to name a few. Materials used for electron emission, such as diamond, diamond-like carbon (DLC) and carbon nanotubes (CNTs) on silicon wafer, have been demonstrated to have possible commercial applications [7–9]. Much effort has been directed in the study of their applications, including their use as electron sources in various visualization equipment, electron beam lithography, electron microscopy, microwave power devices [10–12], and especially for the fabrication of next-generation flat panel displays [13]. To understand quantitatively the physical picture of a single field emitter participating in the field-emission process and the field-emission properties of a single emitter for electron optics applications, accurate measurement of the field emission from an individual emitter is paramount [14].

In the past, several measurement techniques and simulation models have been developed to study the field emission from a single emitter. Gangloff *et al* [15] used the metal-ball anode (250 μm in diameter) to measure the

self-aligned, gate arrays of individual nanotube and nanowire emitters. Bonard [14] measured the field emission of an individual carbon nanotube using a scanning electron microscope (SEM) and found that both the geometry of the carbon nanotube (CNT) and the electrode distance between the CNT and the anode are key factors that affect field emission. Results also indicate that only a small part of an exceptionally long and/or narrow nanotube contributes to the total emitted current in large area measurements. Significant differences exist between the experimental data and the calculated values using the Edgcombe and Valdre model [16], in which the field-enhanced factor (β) correlates empirically with the height and apex radius of the emitter. Based upon these results, these authors believed that the emission process is highly sensitive to the tip structure. Not many details about the measurement technique were revealed in these published studies.

In addition, to understand the field-emission properties of a single emitter, several numerical studies have been conducted to predict field-emission properties. Most of these studies used either a 2D or 3D finite difference method [17–19] or a 2D finite element approach [20] for discretizing the electrostatic Poisson's equation without considering the space–charge effect. However, as the emitter size shrinks down to the nanoscale range, the local electric field at the cathode tip can be very large (up to $\sim$50 V nm^{-1}) for a reasonable magnitude of applied voltage, in which space charges become significant due to a large electron flux, a point that has generally been ignored in previous studies [17–20].

Furthermore, to the best knowledge of the authors, there has been little agreement so far between the experimental and numerical results for field-emission measurements of a single emitter. The reasons may include the following: (1) difficulty in measuring accurately the emission current from a single emitter, especially if the emitter is in the nanoscale range and (2) the limited capability of most numerical models for field emission in both handling complex geometries and taking into account the space–charge effect. In this paper, we attempt to directly measure the field-emission current from a single nano-emitter and compare these results with those from numerical simulation without adjusting any parameters in the model. Since the uniformity and geometry is easier to control than other materials, a silicon nano-emitter array was used as the model emitter to measure the field-emission properties of an individual field emitter. This was done by means of a novel nanomanipulation measurement technique in SEM. At the same time, a parallelized 3D particle-in-cell (PIC) finite element method was used to simulate the field-emission properties of a single emitter, and the results were compared with the experimental data.

2. Experimental method

2.1. Preparation of silicon emitter array and tungsten anode

A crystallized Si(100) wafer (n-type, with 10^{15} cm^{-3} boron doping) was used to form the nanoscale silicon emitter array. This model nanoscale silicon emitter array was fabricated by plasma etching of an inductively coupled plasma (ICP) by means of a three-step process that is depicted in figure 1(a) and described step by step in the following paragraphs.

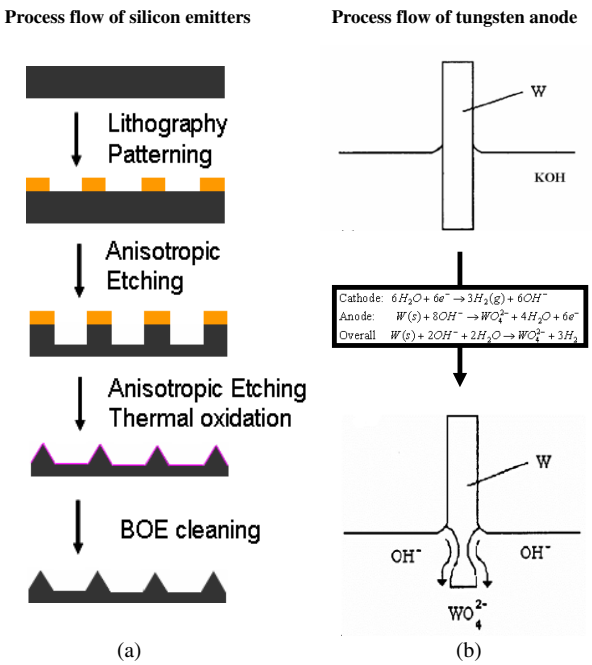

Figure 1. The manufacturing process of (a) a silicon emitter and (b) a tungsten anode.

First, after an RCA clean, a 10 μm circular AZ4620 photoresist mask was patterned by anisotropic ICP etching to produce high aspect ratio circular rods (25 μm in height). Etching was carried out in a commercial vertical reactor (Oxford plasma lab 100) using a mixture of SF_6 and O_2 with high RF power to produce more intense ion bombardment on the wafer.

Second, isotropic etching was used to produce sharp emitters by undercutting the effect under the mask with proper plasma control. For this step, a high SF_6 concentration was necessary to make the isotropic etching by means of the chemical reaction between SF_6 and the silicon rods.

Finally, the silicon tips were placed in the furnace for oxidation, and the silicon oxide was then removed by wet etching using a buffered oxide etching (BOE) solution to form the required nanotip array, as shown in figure 2(a). In addition, wet etching by BOE also ensures that there is no negative oxide layer on the surface of the nanotip. A negative oxide layer degrades the field-emission performance and the reliability of the emitter, potentially making the Fowler–Nordleim (FN) [21] plot nonlinear.

To accurately measure the field-emission properties of a single field emitter, a special tungsten anode was fabricated by electrolysis with a KOH solution, as shown in figure 1(b). *First*, we cut the tungsten filament into a 1 cm long segment and clipped it to the anode of the electrobath. *Second*, we switched on the power supply with enough power so that electrolysis would take place in the KOH electrobath. During this step, light emission occurs due to the reaction between the tungsten filament and the KOH solution. A nanoscale tungsten probe is formed once light emission disappears. As shown in figure 2(b), the typical diameter and apex radius of tungsten anode were 1 μm and 95 nm, respectively. Note that the concentration of the KOH solution is a key factor in controlling

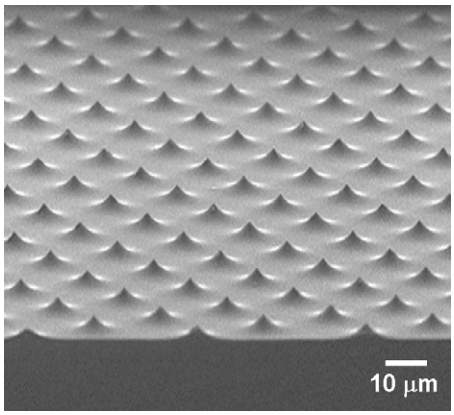

(a)

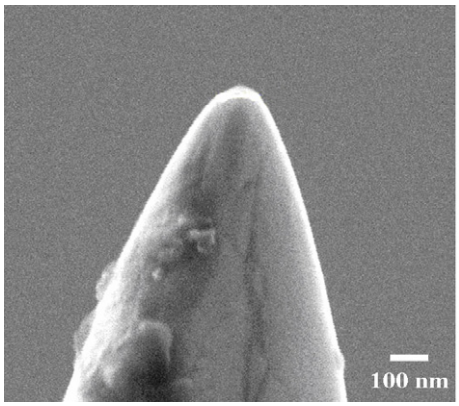

(b)

Figure 2. (a) Typical nanoscale silicon emitter array, (b) typical tungsten anode.

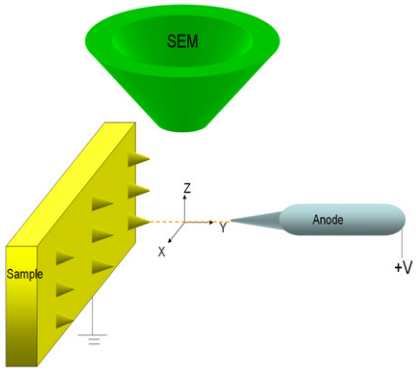

(a)

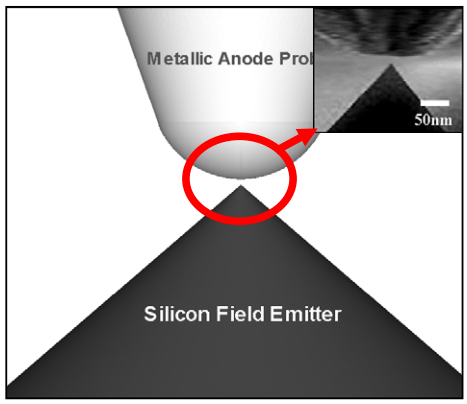

(b)

Figure 3. Typical experimental arrangement of the field-emission measurements. (a) Configuration of the experimental set-up. (b) Sketch of the model nano-emitter with a tungsten anode along with a typical SEM image.

the size of the tungsten anode. In our experiment with a 1 M KOH solution, an applied voltage of 5 V and a current of 30 A were used to fabricate the tungsten nano-anode.

2.2. Nanomanipulation measurements of field-emission properties

Field emission from a single nano-emitter was then measured under a high vacuum condition (9.6×10^{-7} Torr) that can be easily achieved in a standard SEM, as shown in figure 3(a), in which the positions in the X direction and Y direction (the distance between the emitter and the anode) could be controlled to within ± 0.5 nm, using the *in situ* image of SEM. The nanoscale tungsten probe installed on the piezoelectric nanomotor was used as the anode of the silicon nano-emitter. Figure 3(b) shows the model silicon nano-emitter with the tungsten anode, used in the numerical simulation, along with the actual exploded view under the SEM. To accurately measure the emission current from a single nanoscale emitter, we needed to position the tungsten probe precisely, right above the emitter tip. In the present study, a novel experimental technique that can ensure the precise measurement of an emission current was developed and verified by PIC simulation, a process that is described later. The details of this measurement technique are as follows.

First, we focused the nano-emitter apex in the SEM and then moved the tungsten probe in the Y direction such that the distance between the tungsten probe and the emitter tip was maintained at 20 nm. Note that this distance was maintained the same throughout the study, unless otherwise specified. To accurately measure the emission current from the nano-emitter, we needed to identify the shortest distance between the anode (tungsten probe) and the cathode (nano-emitter tip), which was determined by the position of the tungsten probe relative to the emitter tip in the Z direction. Based on the FN law [21], the emission electron flux depends on the local electric field at the cathode, which further varies with the applied voltage, the distance between the anode and the cathode, the work function and the geometry. Thus, a slight deviation from the shortest distance between the anode and the cathode (thus the local electric field) may change the resulting emission current greatly, a point which will be demonstrated in a later section.

Two methods exist, including the *constant voltage* and the *constant emission* modes, by which to position this tungsten probe in the 'right' position in the Z direction. In our study, these two modes were combined to locate the exact position of the tungsten anode. *In the constant voltage mode*, we applied a larger voltage (e.g. 400 V) at the tungsten anode, which was greater than the expected turn-on voltage. Then, the tungsten probe was controlled by the nanomotor to move at a constant speed of 30 nm s^{-1} through a longer distance than for the constant emission mode, and we concurrently measured the emission current to determine the approximate position where

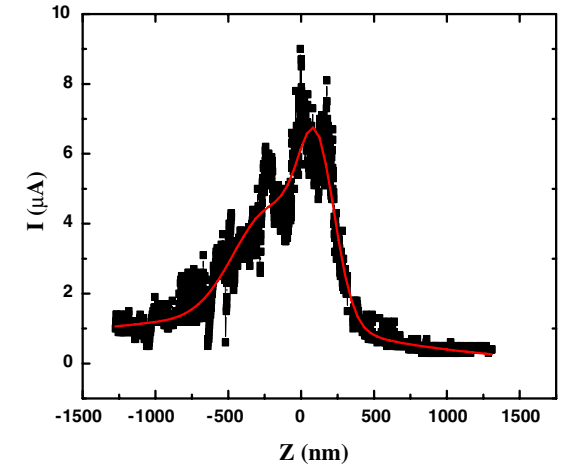

(a)

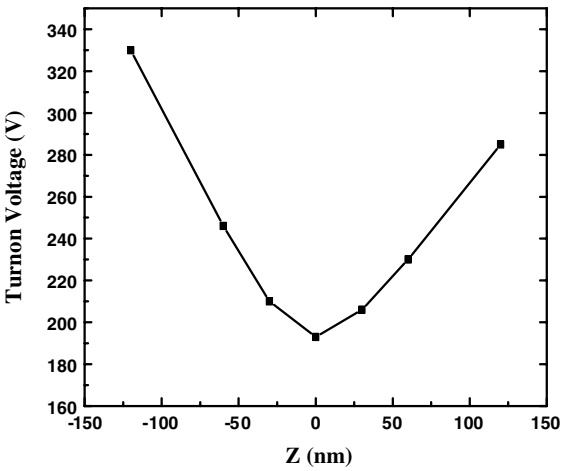

(b)

Figure 4. Methods of positioning the tungsten probe. (a) Constant voltage mode. (b) Constant emission current mode (*turn-on voltage* is defined as the applied voltage across the anode and cathode when the emission current is 1 μA).

the maximum emission current occurs, as shown in figure 4(a). Although this step requires little time, the determined anode position is not precise enough due to the positioning errors caused by the motion-induced vibration. *In the constant emission mode*, we moved the tungsten anode through a shorter distance around the approximate position of the maximum emission current determined in the constant voltage mode and measured the turn-on voltage at each position to find out where the minimum turn-on voltage occurs, as shown in figure 4(b). In this case, the measured minimum turn-on voltage was 193 V, where the emission current was 1 μA. By combining these two steps, we can precisely determine the 'right' position to measure the emission current from a single nano-emitter. Note that this novel technique can be adapted easily to measure the emission current from other types of nanoscale emitters.

3. Numerical method

In the current study, a parallelized 3D PIC code was also developed and applied to simulate the field-emission process from a single silicon tip, and the results were compared with experimental measurements without adjusting any parameters. This simulation code can calculate the instantaneous potential distribution self-consistently by considering the variation and evolution of the charge density in the computational domain during runtime. General procedures for PIC [22] include the following: (1) pushing the particles, (2) assigning charge to surrounding nodes, (3) solving the field equation, (4) interpolating the field (force) to particles, (5) repeating steps (1)–(4). Details of the implementation are described in the following.

The PIC code was modified from a previously developed parallelized 3D Poisson's equation solver with particle ray tracing [23]. This Poisson's equation solver was coupled with a parallelized adaptive mesh refinement module [24], which employed an *a posteriori* error estimator, to automatically refine the mesh near locations with a large electric field. The Poisson's equation was discretized using the Galerkin finite-element method with a linear shape function on an unstructured tetrahedral mesh to provide the flexibility of modelling objects with complex geometry. Parallel implementation for the discretized Poisson's equation solver utilizes a geometrically one-level overlapping preconditioned additive Schwarz method (ASM) [25] with a subdomain-by-subdomain (SBS) scheme [26] using a conjugate gradient algorithm. The particle charge assignment to the neighbouring nodes and the field interpolation from the node to the particles employ the same linear shape function as the one used by the finite-element method (FEM), which automatically conserves the mass and charge. Dynamic load balancing among the processors for the parallelized particle solver applied a multi-level graph-partitioning technique developed previously for the parallelized direct simulation Monte Carlo (DSMC) code [27]. In the *a posteriori* error estimator, we employed a very simple gradient recovery scheme [28] by averaging the cell values of the FE solution to extract the 'exact' solution of the electric field in each cell. A prescribed global relative error ε_{pre} of 0.03% was used to control the level of accuracy throughout the study, unless otherwise specified.

In addition, a Fowler–Nordheim emission model [21] was applied at the cathode surface, which determined the emitted electron flux from the self-consistent electric field solution of Poisson's equation. Based upon the Fowler–Nordheim law, electron flux at the cathode surface in the present study can be written as

$$J = \frac{AE^2}{\phi t^2(y)} \exp\left(-B\frac{\phi^{3/2}}{E} v(y)\right) \text{ A cm}^{-2}, \tag{1}$$

where

$$A = 1.5414 \times 10^{-6}, \tag{1a}$$

$$B = 6.8309 \times 10^{7}, \tag{1b}$$

$$y = 3.79 \times 10^{-4} E^{1/2}/\phi. \tag{1c}$$

Note that E is the local electric field at the emitting surface, y is the image charge lowering the contribution to the work function and ϕ is the work function of the material under study. The functions $t(y)$ and $v(y)$ are approximated by $t^2(y) = 1.1$ and $v(y) = 0.95 - y^2$. In general, emitted electron flux increases with increasing local electric field, which reduces

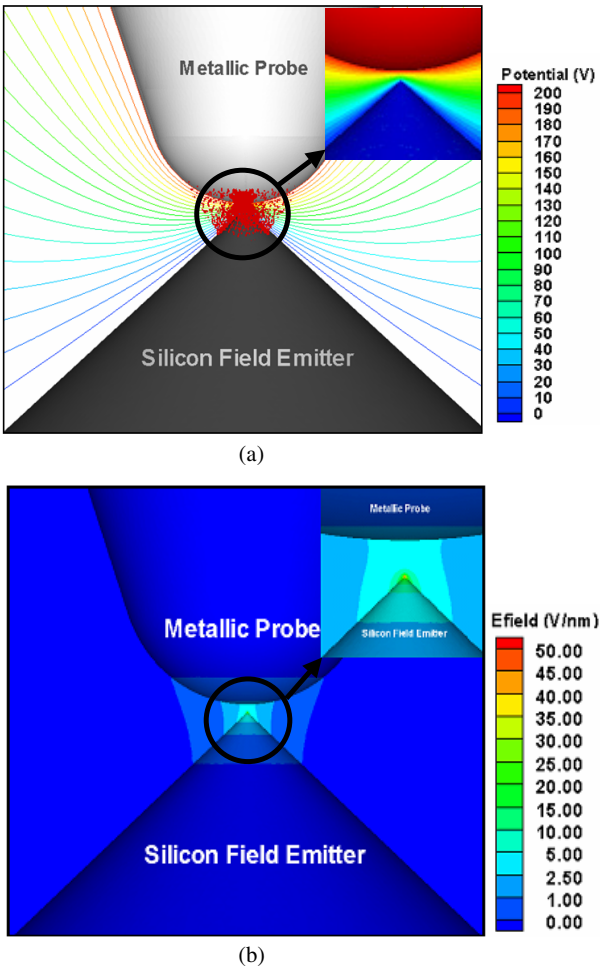

Figure 5. Simulated property distribution in the exploded view near the nano-emitter tip. (a) Potential along with snapshot of electrons. (b) Electric field.

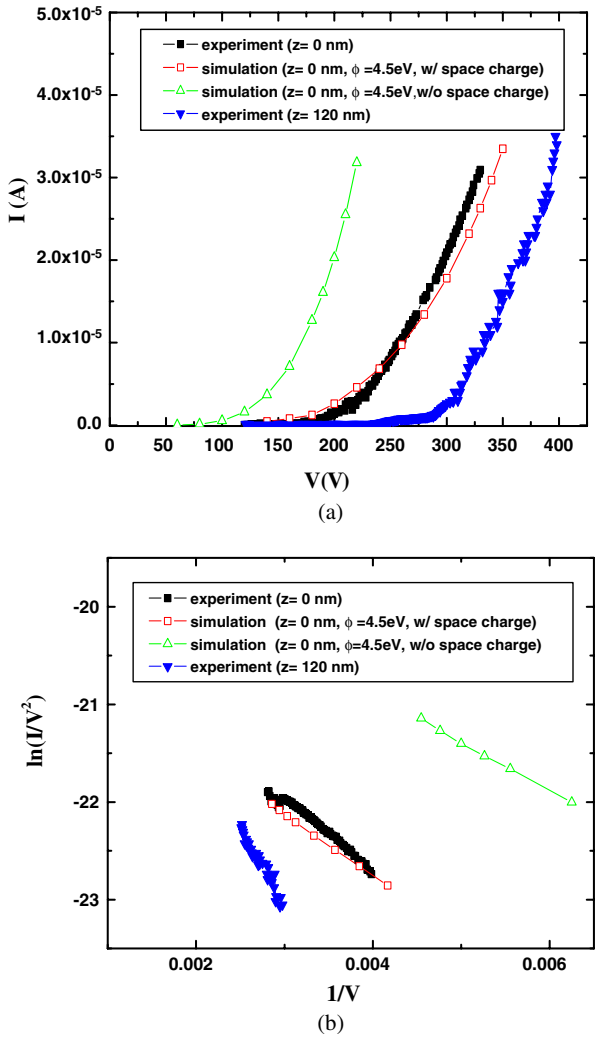

Figure 6. Comparison of the experimental and simulated current–voltage curves (work function = 4.5 eV). (a) Linear I–V curve. (b) FN plot.

the barrier width for tunnelling, while it decreases with increasing work function, which augments the barrier height for tunnelling. In our experiment, an n-type silicon wafer with 10^{15} cm^{-3} doping was used to manufacture our emitter as mentioned earlier. The work function ϕ can then be estimated [29] to be approximately 4.5 eV. Thus, we used $\phi = 4.5$ eV in our simulation throughout the study. The electron trajectory from the emitter surface to the anode surface was integrated and traced on the unstructured mesh, using self-consistent electric field distribution from the Poisson's equation solver, in addition to the cell-by-cell particle tracking technique developed previously for DSMC simulation [30]. The emission current was then computed as the time average of the accumulated electron charges reaching the anode surface.

4. Results and discussion

The nano-emitter model is shown schematically in figure 3(b). Simulation conditions include cathode-to-anode distance = 20 nm, applied voltage = 130–350 V, ~100 000 nodes (after refinement), ~600 000 tetrahedrons (after refinement) and timestep = 1×10^{-18} s. Figure 5 shows the simulated property distribution considering the space–charge effect. Figure 5(a) illustrates the steady-state potential distribution along with a snapshot of the emitted electrons. At steady state, there were approximately 3000 electrons in the computational domain. Most of the electrons were emitted from the tip region having very high electric field (up to ~50 V nm^{-1}), which is shown in figure 5(b) as an exploded view.

Figure 6(a) shows the comparison between the experimental and simulated I–V curves, while figure 6(b) shows the corresponding FN plot. In figure 6(a), the simulated emission currents for the case where the space–charge effect was taken into account compared very well with those observed experimentally; conversely, those generated without considering the space–charge effect generally appear much larger than those from the experiments. A reduced emission current, relative to the case that did not account for the space–charge effect, results from the emitted electron clouds near the cathode (tip) surface. This reduction in the emission current reduces the local electric field at the tip surface or equivalently the shielding effect due to the charge particles. Therefore, our experimental and

simulation data both clearly demonstrate that the space–charge effect due to the emitted electrons is important in determining the field-emission current from a nano-emitter in the present configuration.

Furthermore, the simulated turn-on voltage, which is defined as the applied voltage leading to a current of 1 μA, was 175 V, which deviates only 9.3% from the experimental value of 193 V. In addition, another measured I–V curve in figure 6(a) with $z = 120$ nm deviates considerably from the correct one, revealing that the results are very sensitive to positioning accuracy, which highly justifies the novel positioning technique developed in the present study. The corresponding field enhancement factor, β, which relates the applied averaged electric field (V/d, V: applied voltage, d: anode-to-cathode distance) to the local electric field at the nanotip, can be easily found from figure 6(b) to be 2.495 and 2.224 for experiments and simulations, respectively. Moreover, the single slope in figure 6(b) clearly indicates that the field emission from a silicon emitter is a typical barrier-tunnelling, quantum mechanical process [31].

5. Conclusions

In summary, we successfully investigated the field-emission characteristics of a single silicon nanotip by means of nanomanipulation measurements and PIC modelling. In our study, a novel measurement technique was developed to determine the 'right' position in which to measure the emission current from a single nano-emitter. Using this measurement technique, the experimentally observed characteristics, including the I–V curve, turn-on voltage and field enhancement factor, all coincided very well with the PIC simulations for the case that considered the space–charge effect due to the emitting electrons. Simulation and experimental results for the turn-on voltage show less than a 9.3% difference. The results also reveal that the field emission from a single silicon tip is a typical barrier-tunnelling, quantum mechanical process.

Acknowledgments

The authors would like to thank Dr Volker Klocke and Dr Andreas Rosenberger, now at the Klocke Nanotechnik, for their technical support. We are also grateful to Mr Frank Mak at Tricopek for his encouragement and helpful discussions. In addition, the financial support to the corresponding author, JSW, by National Science Council of Taiwan through 95-2221-E-009-018 is highly appreciated.

References

[1] Ng K L, Yuan J, Cheung J T and Cheah K W 2002 *Solid State Commun.* **123** 205
[2] Nillson L, Groening O, Emmenegger C, Kuettel O, Schaller E and Schlapbach L 2000 *Appl. Phys. Lett.* **76** 2071
[3] Temple D 1999 *Mater. Sci. Eng. Rep.: Rev. J.* **24** 185
[4] Merkulov V I, Lowndes D H and Baylor L R 2001 *J. Appl. Phys.* **89** 1933
[5] Guillorn M A, Melechko A V, Merkulov V I, Hensley D K, Simpson M L and Lowndes D H 2002 *Appl. Phys. Lett.* **81** 3660
[6] Guillorn M A, Melechko A V, Merkulov V I, Ellis E D, Britton C L, Simpson M L, Lowndes D H and Baylor L R 2001 *Appl. Phys. Lett.* **79** 3506
[7] Brodie I and Spindt C A 1992 *Adv. Electron Electron Phys.* **83** 1
[8] Holland C E, Rosengreen A and Spindt C A 1991 *IEEE Trans. Electron Devices* **38** 2368
[9] Schwoebel P R and Brodie I 1995 *J. Vac. Sci. Technol.* B **13** 1391
[10] Spindt C A, Brodie I, Humphrey L and Westerberg E R 1976 *J. Appl. Phys.* **47** 5248
[11] Rakhshandehroo M R, Weigold J W, Tian W C and Pang S W 1998 *J. Vac. Sci. Technol.* B **16** 2849
[12] Rakhshandehroo M R and Pang S W 1999 *IEEE Trans. Electron Devices* **46** 792
[13] Smith R C, Co D C and Silva S R P 2005 *Appl. Phys. Lett.* **87** 103112
[14] Bonard J M, Dean K A, Coll B F and Klinke C 2002 *Phys. Rev. Lett.* **89** 197602
[15] Gangloff L *et al* 2002 *Nano Lett.* **4** 1575
[16] Edgcombe C J and Valdré U 2002 *Phil. Mag.* B **82** 987
[17] Wang C, Wang B and Zhao H 1997 *J. Vac. Sci. Technol.* B **15** 394
[18] Lei W, Wang B and Yin H 1998 *J. Vac. Sci. Technol.* B **16** 2881
[19] Hu Y and Huang C H 2003 *J. Vac. Sci. Technol.* B **21** 1648
[20] Hong M A 1994 *J. Vac. Sci. Technol.* B **12** 764
[21] Fowler R H and Nordheim L 1928 *Proc. R. Soc.* A **119** 173
[22] Birshall C K 1991 *IEEE Trans. Plasma Sci.* **19** 65
[23] Hsu K H, Chen P Y, Hung C T, Chen L H and Wu J S 2006 *Comput. Phys. Commun.* **174** 948
[24] Lian Y Y, Hsu K H, Shao Y L, Lee Y M, Jeng Y W and Wu J S 2006 *Comput. Phys. Commun.* **175** 721
[25] Hwang F N and Cai X C 2005 *J. Comput. Phys.* **205** 666
[26] Saad Y 2003 *Iterative Methods for Sparse Linear Systems* (Philadelphia, PA: Society for Industrial and Applied Mathematics)
[27] Wu J S and Tseng K C 2005 *Int. J. Numer. Methods Eng.* **63** 37
[28] Zienkiewicz O C and Chu J Z 1987 *Int. J. Numer. Methods Eng.* **24** 337
[29] Sze S M 1985 *Physics of Semiconductor Devices* (New York: Wiley)
[30] Wu J S and Lian Y 2003 *Comput. Fluids* **32** 1133
[31] Morales A M and Lieber C M 1998 *Science* **279** 208